RSC Advances

PAPER

View Article Online
View Journal | View Issue

Cite this: *RSC Adv.*, 2019, **9**, 12696

A magnetically recyclable superparamagnetic silica supported Pt nanocatalyst through a multi-carboxyl linker: synthesis, characterization, and applications in alkene hydrosilylation†

Laiming Li, Youxin Li,* Jincong Yan, Hang Cao, Dongyun Shao and James J. Bao

To simplify separation procedures, improve the reusability and decrease the loss of Pt, two Pt catalysts anchored on superparamagnetic silica (Fe_3O_4@SiO_2-EDTA@Pt and Fe_3O_4@SiO_2-DTPA@Pt) were prepared for the first time. The stable magnetic properties made them easily recyclable using a magnet rather than filtration, decantation or centrifugation. After 12 catalytic runs for both 30–50 nm Pt catalysts, the yield of 1-heptylmethyldichlorosilane was still up to 90%. The average loss of Pt in each reaction was only 0.87% for Fe_3O_4@SiO_2-EDTA@Pt and 0.66% for Fe_3O_4@SiO_2-DTPA@Pt owing to the strong interaction between Pt and carboxyl. The unprecedented activity and selectivity of the two Pt nanoparticle catalysts were observed in the hydrosilylation of alkenes. The turnover number in the reaction between 1-hexene and methyldichlorosilane using 5×10^{-8} mol of the Pt approached 662 733 for Fe_3O_4@SiO_2-EDTA@Pt and 579 947 for Fe_3O_4@SiO_2-DTPA@Pt over 12 h. The corresponding hydrosilylation products in excellent yields were obtained when we employed a broad range of alkenes as substrates, including 5 isomerous hexenes and 14 important industry raw materials. Fe_3O_4@SiO_2-DTPA@Pt showed a better activity. They have potential for catalyzing more reactions and replacing the current homogeneous Pt catalysts in industry.

Received 16th January 2019
Accepted 26th March 2019

DOI: 10.1039/c9ra00375d

rsc.li/rsc-advances

1. Introduction

Magnetic materials such as magnetite (Fe_3O_4) and maghemite (γ-Fe_2O_3) are widely utilized in various fields, such as high-density data storage, chemical sensors, catalysts, drug delivery, biological assays, and electro photographic developers.[1–5] Compared with traditional techniques such as filtration, decantation or centrifugation, magnetic materials could be easily separated from solution and re-dispersed through an external magnetic field,[6] which overcomes time- and solvent-consuming procedures.[6] Magnetite Fe_3O_4, especially nano-Fe_3O_4 possessing super paramagnetic behavior at a nanoparticle size with high surface area, is attractive for practical applications.[7–10] An ongoing application of magnetic materials is to immobilize metal catalysts because efficient separation, recovery and recycling of the catalyst may enhance their lifetime and minimize their consumption to result in significant economical and environmental benefits.[11–14]

Among these transition metal catalysts, such as copper (Cu), platinum (Pt), palladium (Pd), rhodium (Rh), nickel (Ni) or ruthenium (Ru),[15–20] Pt is one of the most widely used owing to its unparalleled catalytic activity and mild reaction conditions in various fields, such as hydrosilylation, aldehyde oxidation, sulfuric acid decomposition. Although homogeneous Pt catalysts such as Speier's catalyst and the Karstedt's catalyst suffer from a number of drawbacks, like side reactions and low selectivity and reusability, there isn't efficient substitution in industry. The immobilization of platinum catalyst is a wise choice. Numerous researches were being reported on how to immobilize Pt on magnetic materials.[21–26]

Magnetic silica is used as an ideal inorganic support because of its merits, like magnetic property, easy modification, high biocompatibility, solvent compatibility, adsorption capacity, acid–base properties, and chemical and thermal stability when compared to other structures.[27–29] A number of multi-carboxyl based affinity ligands, such as ethylenediaminetetraacetic acid (EDTA) and diethylenetriaminepentaacetic acid (DTPA), are well-known chelators for their strong metal-complexing property.[30] Magnetic silica particles modified by EDTA or DTPA were widely used in industries including cleaning, the nuclear industry, pharmaceuticals, and the manufacturing of textile leather, rubber, and paper, *etc.*[31–35] The immobilized Pt catalysts on silica gel through EDTA and DTPA were developed by our

Tianjin Key Laboratory for Modern Drug Delivery and High-Efficiency, Collaborative Innovation Center of Chemical Science and Engineering, School of Pharmaceutical Science and Technology, Tianjin University, Room 412-8, Building No. 24, 92 Weijin Road, Nankai District, Tianjin 300037, China. E-mail: lyx@tju.edu.cn; Fax: +86-22-2789-2820; Tel: +86-22-2789-2820

† Electronic supplementary information (ESI) available. See DOI: 10.1039/c9ra00375d

group.[36,37] EDTA and DTPA showed a strong interaction with platinum, but the kinds of heterogeneous catalysts still need to reuse through centrifugation and 31% Pt was loss after 13 recycles.

Here, we first time try to immobilize Pt catalysts through carboxyl ligands like EDTA or DTPA grafted onto the surface of magnetite silica (Fe_3O_4@SiO_2-EDTA@Pt and Fe_3O_4@SiO_2-DTPA@Pt) to simplify separation procedure, improve the reusability and decrease the loss of Pt. In addition, the two catalysts are applied first time in 4 isomerization–hydrosilylation and hydrosilylation of 14 compounds, which are important industry raw materials. These make the current two catalysts more valuable industry.

2. Experimental section

2.1. Materials and reagents

All chemicals were used as received without further purification. Iron chloride hexahydrate ($FeCl_3 \cdot 6H_2O$, >99%) and ferrous chloride tetrahydrate ($FeCl_2 \cdot 4H_2O$, >99%) were from Yuanli Chemical. γ-Aminopropyltrimethoxysilane (APTMS) was from Qufu Chenguang Chemical. Tetraethylorthosilicate (TEOS) was from Tianjin Kemiou Chemical Reagent. Ethylenediaminetetraacetic acid (EDTA), diethylenetriaminepentaacetic acid (DTPA), sodium silicate, ammonia solution (25%), anhydrous pyridine, acetic anhydride, diethyl ether, hydrochloric acid (HCl), toluene, acetone, ethanol, methanol, *n*-decane, i-propanol, *n*-butanol and *n*-hexanol were from Jiangtian Chemical Technology. Methyldichlorosilane was from Kaihua Synthetic. 1-Hexene, *trans*-2-hexene, *cis*-2-hexene, *trans*-3-hexene and *cis*-3-hexene were form Tokyo Chemical Industry Co., Ltd. *N*,*N*-Dimethylacrylamide, 1,2-epoxy-4-vinylcyclohexane, methyl methacrylate, butyl acrylate, ethane-1,2-diyl bis(2-methylacrylate), crotonic acid ethyl ester and *trans*-2-hexenyl acetate were from Bid Pharmatech Ltd. 1,2-Epoxy-7-octene, allyl glycidyl ether, 5-hexen-2-one, allylchloride and *trans*-2-hexen-1-yl phenylacetate were from Nanjin Shengbicheng Chemical Technology Co., Ltd. Cyclohexene and norbornylene were from Shanghai Macklin Biochemical Co., Ltd. $H_2PtCl_6 \cdot 6H_2O$ was from Tianjin Fengchuan Chemical Reagent Technologies. 1-Hexyl-methyldichlorosilane was from CNW Technologies. Deionized water was from Tianjin Yongyuan Distilled Water Manufacturing Center.

2.2. Materials synthesis

2.2.1. Preparation of Fe_3O_4 and Fe_3O_4@SiO_2. The magnetite Fe_3O_4 and Fe_3O_4@SiO_2 nanoparticles were prepared according to previous reported method with a minor modification.[38–43] The magnetite Fe_3O_4 nanoparticles were prepared by chemical co-precipitation of ferric and ferrous ions in ammonium hydroxide solution. Briefly, under nitrogen protection, 0.04 mol $FeCl_3 \cdot 6H_2O$ and 0.02 mol $FeCl_2 \cdot 4H_2O$ were dissolved in distilled water with vigorous stirring at 80 °C for 20 min. After 15 mL ammonium hydroxide (25% aqueous solution) was added to the solution, the color of the bulk solution turned from orange to black immediately. After 30 min of reaction, the black precipitate was collected from the reaction mixture by a powerful magnet and washed three times with distilled water before it was re-dispersed into a 100 mL distilled water to form a nanoparticle suspension of *ca.* 50 mg mL^{-1}.

The magnetite Fe_3O_4@SiO_2 nanoparticles were prepared by two sol–gel approach. First, the surface of Fe_3O_4 nanoparticles was covered by silica layer (SiO_2 encapsulated Fe_3O_4 particles, Fe_3O_4@SiO_2). Briefly, sodium silicate was dissolved in deionized water in a glass beaker equipped with a mechanical stirrer and the pH was adjusted to 12–13 by sodium hydroxide. Fe_3O_4 nanoparticles were added to the sodium silicate solution. The mixture was treated ultrasonically for 30 min. Then, the temperature of the mixture was increased to 85 °C and nitrogen gas was used to prevent the intrusion of oxygen. 2 M hydrochloric acid was added dropwise to adjust pH value to 6.0. Then, the precipitates were washed several times with deionized water by magnetic decantation. The Fe_3O_4@SiO_2 was coated again to ensure that the desired amount of silica on all magnetite Fe_3O_4.[44,45] For this, Fe_3O_4@SiO_2 was re-dispersed in 100 mL methanol–water (1 : 1, v/v) mixture and followed by the addition of 1 mL ammonium hydroxide (25% aqueous solution). Then, 1 mL of TEOS was dissolved in 10 mL methanol and added dropwise to the mixture by gently stirring for 1 h. The obtained nanoparticles (Fe_3O_4@SiO_2) were collected by magnet and washed several times with distilled water and ethanol. Finally, the nanoparticles were dried at room temperature under vacuum and brown yellow solid was observed.

2.2.2. Preparation of amino-magnetic silica (Fe_3O_4@SiO_2-AP). It was prepared according to previous reported method.[46] Ten grams as-made magnetic silica nanoparticles were ultrasonically dispersed in 100 mL distilled toluene for 30 min. Then, it was transferred into a 250 mL three-necked flask equipped with a mechanical stirrer. 3-Aminopropyltrimethoxysilane (20 mL) was added into this mixture. The temperature was kept at 110 °C with continuous stirring for 24 h. The resulting nanoparticles were separated by magnet, washed with methanol for several times and then dried at 60 °C under vacuum for 12 h. The product was referred to as Fe_3O_4@SiO_2-AP.

2.2.3. Preparation of multi-carboxyl magnetic silica (Fe_3O_4@SiO_2-EDTA and Fe_3O_4@SiO_2-DTPA). The preparation of EDTA or DTPA dianhydride was done according to a previous reported method with minor modification.[47] EDTA or DTPA was suspended in pyridine followed by the addition of acetic anhydride. The mixture was stirred at 65 °C for 24 h. The product was filtered, washed with acetic anhydride and diethyl ether, and dried in an oven for 6 h. Next, 5 g of Fe_3O_4@SiO_2-AP was suspended in 100 mL mixture solution of ethanol and acetic acid (1 : 1, v/v). After the addition of 25 g of EDTA dianhydride or 30 g DTPA dianhydride, the mixture was kept at 80 °C for 24 h to allow the amino groups on the silica gel to react with the carboxyl groups.[48,49] Finally the yellowish-brown product was separated by magnet and washed with 4 M ammonia water solution to remove unreacted EDTA or DTPA.[50] Then products were washed again with ethanol/acetic acid (1 : 1, v/v), water and methanol sequentially.[51] The multi-carboxyl modified

magnetic silica gels (Fe_3O_4@SiO_2-EDTA or Fe_3O_4@SiO_2-DTPA) were dried in an oven at 90 °C for 8 h.

2.2.4. Preparation of catalysts. The above multi-carboxyl modified magnetic silica gels (Fe_3O_4@SiO_2-EDTA or Fe_3O_4@SiO_2-DTPA) (1.51 g) were added to 50 mL $H_2PtCl_6 \cdot 6H_2O$ (0.20 g) ethanol solution. The mixture was carried out in a reflux at 80 °C under nitrogen atmosphere and stirred for 9 h. The solid product was filtered by a magnet and washed with ethanol successively and dried at 70 °C for 3 h. The light yellow platinum complex was obtained, which were denoted as Fe_3O_4@SiO_2-EDTA@Pt and Fe_3O_4@SiO_2-DTPA@Pt. The process was schematically illustrated in Fig. 1.

2.3. Characterization of the catalysts

The crystal lattice structure of the magnetic intermediates (Fe_3O_4, Fe_3O_4@SiO_2, Fe_3O_4@SiO_2-AP), and products (Fe_3O_4@SiO_2-EDTA@Pt, Fe_3O_4@SiO_2-DTPA@Pt) were identified by XRD, in the 2θ range of 10–90° at a scan speed of 4° min^{-1}, using a Rigaku D/MAX-2500 diffractometer with Cu-Kα radiation (λ = 0.1540 nm). Particle sizes of the catalysts were studied using a JEOL JEM-2100F apparatus with an accelerating voltage of 200 kV. TEM of Fe_3O_4@SiO_2-EDTA@Pt, Fe_3O_4@SiO_2-DTPA@Pt were prepared by placing a drop containing the nanoparticles in a coated carbon grid. The morphology of the catalysts was investigated using a Hitachi S2800 SEM. The EDS analysis, which was simultaneously performed during the SEM examinations, was conducted to confirm the element distribution on the surface of adsorbents. FT-IR spectra were taken in KBr pressed pellets on a TENSOR 27 Spectrometer. EA was used to measure the nitrogen content in the materials on an Elementar Vario Micro cube. The thermal stabilities were measured by TGA employing a NETZSCH STA 409 TG-DTA under a dynamic nitrogen atmosphere at a heating rate of 10 °C min^{-1}. The magnetization and hysteresis loops were measured at room temperature by a LDJ9600 VSM. The BET measurement was carried out on a Quantachrome NOVA 1000 system at liquid-N_2 temperature.

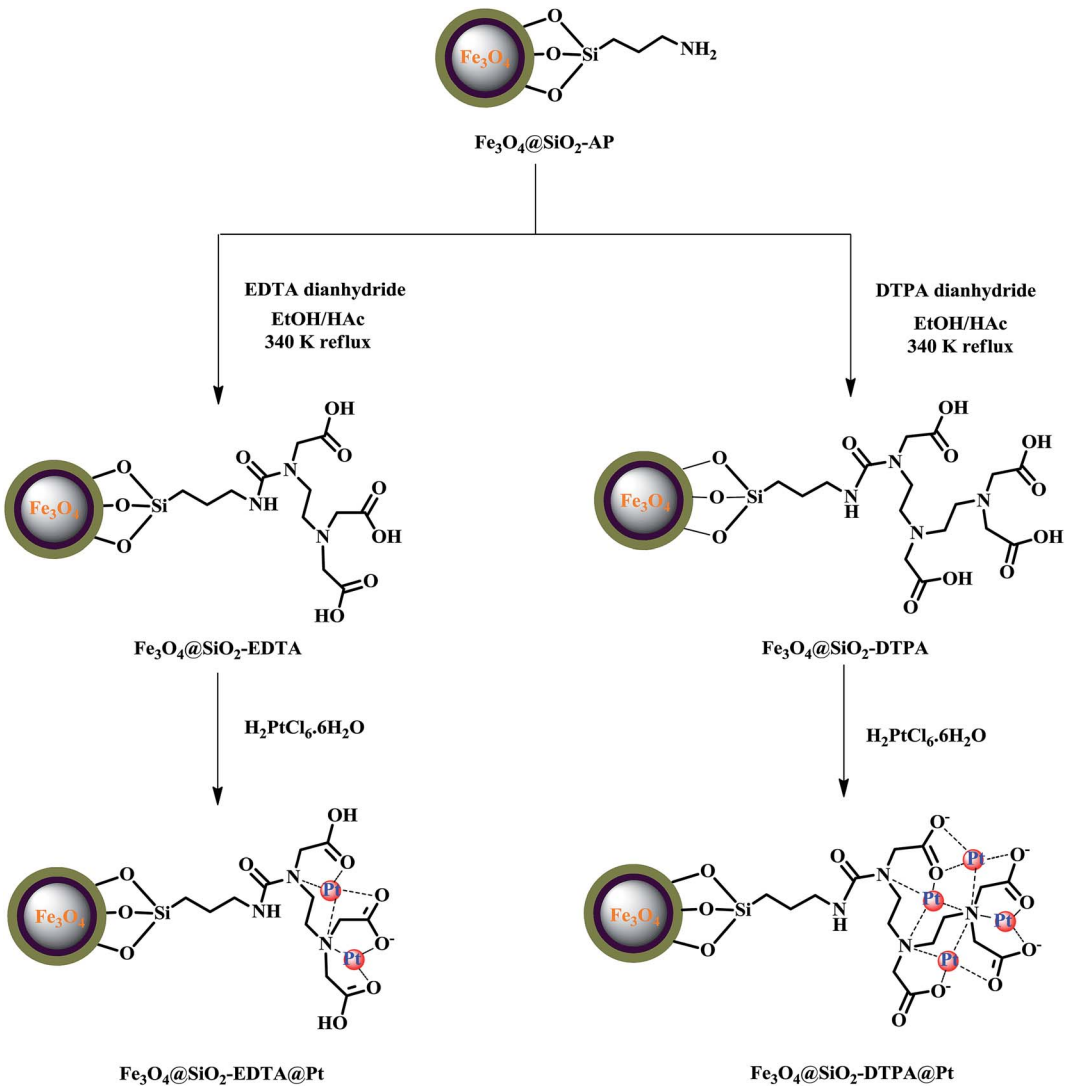

Fig. 1 Preparation of Fe_3O_4@SiO_2-EDTA@Pt and Fe_3O_4@SiO_2-DTPA@Pt catalysts.

2.4. Catalytic alkene hydrosilylation

In a general procedure, hydrosilylation was carried out in a 50 mL round-bottomed tube equipped with a homemade reflux condenser to the upper of which a heating system was attached. An appropriate amount of alkene and platinum magnetic complex were stirred at a specific reaction temperature for 30 min before 15 mmol methyldichlorosilane was added. The structure and yield of hydrosilylation products were determined based on calibration curves of standards. The catalyst was collected by simple magnetic separation and reused in subsequent runs without any treatment. All hydrosilylation products were characterized by comparing their spectra and physical parameters with authentic samples. The reaction product was quantified by gas chromatography (GC) and the structures of products were identified by nuclear magnetic resonance (NMR). GC equipped with a flame ionization detector (FID) (Wuhan Trustworthy Technology, China) and a long capillary column (30 m × 0.25 mm × 0.25 μm) coated by 5% phenyl and 95% methyl polysiloxane. Injector and detector temperature was 260 °C, carrier gas was nitrogen, injection volume at 0.8 μL, temperature programme: the column was kept at 60 °C for 3 min, then heated to 260 °C at a rate of 10 °C min^{-1}. ^1H NMR spectra were recorded on a Bruker AC-P400 (400 MHz) spectrometer in $CDCl_3$ as solvent.

3. Results and discussion

3.1. Synthesis

In the synthetic procedures described earlier, magnetite Fe_3O_4 nanoparticles were prepared by the co-precipitation method from ferrous and ferric ion solutions at a mol ratio of 1 : 2. The magnetic nanoparticles have extensive hydroxyl groups on its surface when contacted with aqueous phase.[52] Silicic acid as silica precursors encapsulated the Fe_3O_4 nanoparticles by two sol–gel approaches. First silicate acid layer was formed gradually from sodium silicate solution by dropwise addition of hydrochloric acid. The second silicate acid layer was formed by dropwise addition of TEOS solution. However, the TEOS is non-polar in nature and it is necessary to use organic reagent like methanol as a mutual solvent to make TEOS and water miscible. Subsequently, the silanol groups (Si–OH) on the surface are transformed into siloxane bonds (Si–O–Si) *via* the condensation reaction and the silica coating is formed.[53] Notably, the introduction of a dense silica coating on the magnetic nanoparticles is necessary for this study. It protects the magnetic Fe_3O_4 from oxidation and provides the surface charges needed to prevent aggregation in the subsequent condensation reactions and practical applications. The silanol groups change the surface properties making it easier and more effective to perform surface modification with organic silane molecules.

Before being modified by EDTA or DTPA group, the magnetic silica nanoparticles were functionalized with APTMS, which acted as an auto-catalyst. Those amino groups on the magnetic silica surface enable the magnetic silica materials to be functionalized with EDTA and DTPA by grafting the corresponding anhydrides on those amino groups. The EDTA or DTPA groups, in turn, serve as a new matrix to immobilize metallic Pt. The chemical structures of the resulting product were depicted in Fig. 1. The multi-carboxyl functionalized magnetic silica materials were found to be a yellow powder with an excellent shelf life. These magnetite nanoparticles functionalized with EDTA or DTPA will be referred to as Fe_3O_4@SiO_2-EDTA@Pt and Fe_3O_4@SiO_2-DTPA@Pt.

3.2. Characterization

The data from AAS analysis indicated the amounts of Pt in Fe_3O_4@SiO_2-EDTA@Pt and Fe_3O_4@SiO_2-DTPA@Pt were 173.80 and 192.77 μmol g^{-1}, respectively. As a comparison, Pt was also immobilized on Fe_3O_4@SiO_2-AP and Fe_3O_4@SiO_2, which had only 33.40 and 0.10 μmol g^{-1} of Pt, respectively. It means the interaction between Pt and carboxyl is stronger than amino group, which is benefit to the immobilization and stability of Pt.

Morphology of the two novel catalysts was characterized by SEM, EDS and TEM (Fig. 2). Results showed that the dried power of Fe_3O_4@SiO_2-EDTA@Pt and Fe_3O_4@SiO_2-DTPA@Pt nanoparticles had an irregular surface with sharp edge and slight agglomeration, which could be dispersed well in solution. The presence of Si, O and Fe signals in the EDS pattern confirmed that Fe_3O_4 was successfully mixed with silica. The higher intensity of Si peak compared with that of Fe peak showed that the Fe_3O_4 nanoparticles were coated by SiO_2. The collected process by a magnet avoids the SiO_2 nanoparticles without Fe_3O_4. The EDS analysis results also confirmed the elemental composition of the nanoparticles and the existence of Pt in the prepared nanoparticle catalysts. Through second robust sol–gel approach, the high magnification TEM images revealed that the Fe_3O_4@SiO_2-EDTA@Pt and Fe_3O_4@SiO_2-DTPA@Pt particles obtained were uniform with a diameter of about 30–50 nm. Each magnetic particle was composed of dark magnetic Fe_3O_4 nanoparticles of about 10–15 nm diameter. Even further, it clearly showed that those dark magnetic particles were coated with a light-gray SiO_2 layer with a thickness of around 15 nm.

The XRD patterns of Fe_3O_4, Fe_3O_4@SiO_2, Fe_3O_4@SiO_2-AP, Fe_3O_4@SiO_2-EDTA@Pt and Fe_3O_4@SiO_2-DTPA@Pt nanoparticles were shown in Fig. 3. It showed typical X-ray diffraction patterns of Fe_3O_4.[54] The characteristic diffraction peaks appeared in Fe_3O_4 at 30.1°, 35.5°, 43.3°, 54.3°, 57.3° and 62.6° could be assigned to the planes of Fe_3O_4 (JCPDS No. 19629), respectively. These characteristic diffraction peaks were observed in Fe_3O_4@SiO_2, Fe_3O_4@SiO_2-AP, Fe_3O_4@SiO_2-EDTA@Pt and Fe_3O_4@SiO_2-DTPA@Pt nanoparticles which indicated that Fe_3O_4 was existent in all synthesized samples and the whole preparation processes did not result in the phase change of Fe_3O_4. The obvious characteristic peak of Pt wasn't observed in Fe_3O_4@SiO_2-EDTA@Pt and Fe_3O_4@SiO_2-DTPA@Pt, which may indicate that the amount of Pt was low or the Pt particles were highly dispersed on the surface of support.[55]

In order to confirm properties of the surface of composite nanoparticles, the molecular structure of the different composites was characterized using FT-IR spectra (Fig. 4.). The typical absorption peak for Fe_3O_4 at 635 and 576 cm^{-1} was

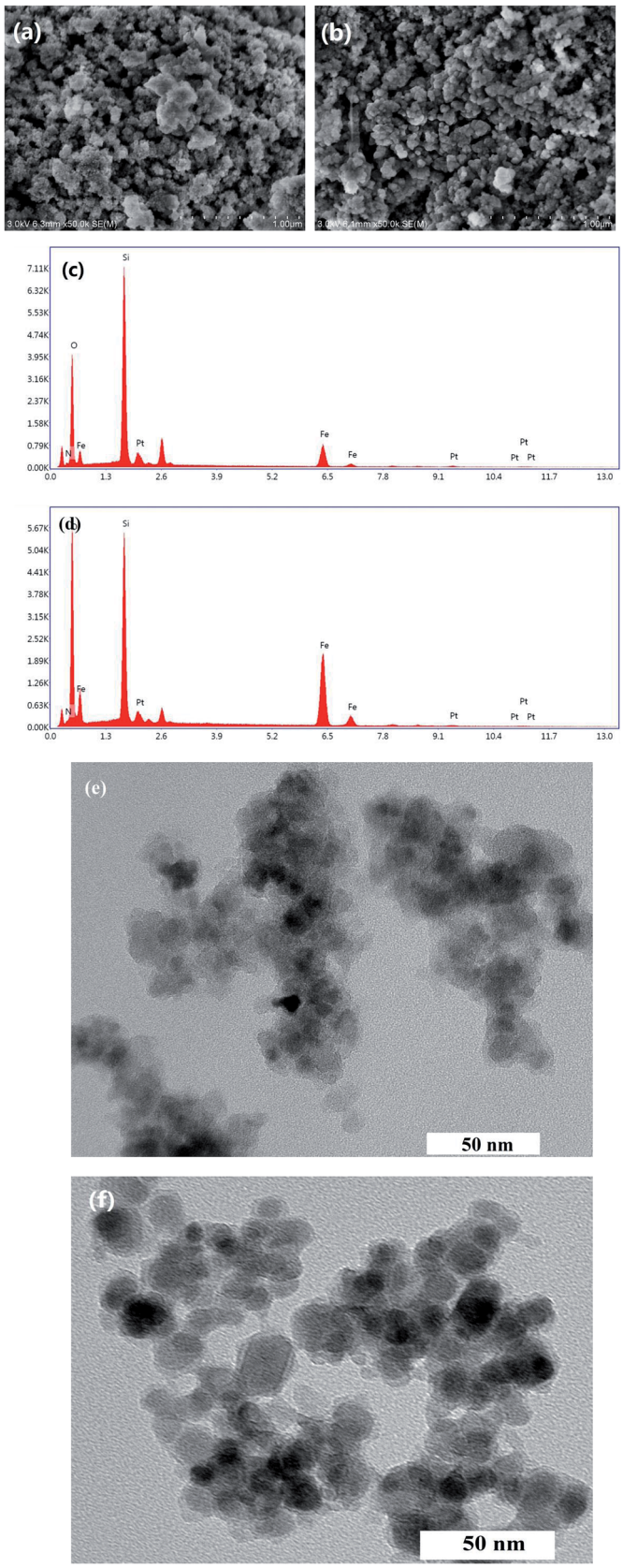

Fig. 2 SEM micrographs of (a) Fe_3O_4@SiO_2-EDTA@Pt and (b) Fe_3O_4@SiO_2-DTPA@Pt, EDS of (c) Fe_3O_4@SiO_2-EDTA@Pt and (d) Fe_3O_4@SiO_2-DTPA@Pt, TEM micrographs of (e) Fe_3O_4@SiO_2-EDTA@Pt and (f) Fe_3O_4@SiO_2-DTPA@Pt.

attributed to the stretching vibration of Fe–O bond. The typical peaks of Fe_3O_4 were observed in all of spectra, which further confirmed Fe_3O_4 nanoparticles existed in all of intermediates and products. Whereas the gradual decrease of peak signals indicated the Fe_3O_4 nanoparticles were at core of Fe_3O_4@SiO_2, Fe_3O_4@SiO_2-AP, Fe_3O_4@SiO_2-EDTA, Fe_3O_4@SiO_2-EDTA@Pt, Fe_3O_4@SiO_2-DTPA and Fe_3O_4@SiO_2-DTPA@Pt. For Fe_3O_4@SiO_2, a new board absorption peak at 1092 cm^{-1} resulted from Si–O–Si antisymmetric stretching vibration of silica layer, which verified the successful coating of silica layers onto Fe_3O_4.[56,57] The peak around 1627 cm^{-1} was attributed to the absorbed water on the silica shell or the silanol group of the silica.[58] The characteristic absorption band at 3422 cm^{-1} was from the stretching vibrations of hydroxyl groups. These peaks from Fe_3O_4@SiO_2 were also observed in Fe_3O_4@SiO_2-AP, Fe_3O_4@SiO_2-EDTA, Fe_3O_4@SiO_2-DTPA, Fe_3O_4@SiO_2-EDTA@Pt and Fe_3O_4@SiO_2-DTPA@Pt. After the functionalization of Fe_3O_4@SiO_2 with APTMS, the new absorption peaks at 2925 and 2858 cm^{-1} represented the symmetric vibrations of aliphatic C–H stretching of the methylene group for silane coupling agent, which indicated that amino group was successfully grafted onto the surface of Fe_3O_4@SiO_2. After grafting multi-carboxyl groups, the strong characteristic absorption band appeared at 1733 and 1404 cm^{-1} could be assigned to C=O and C–O stretching vibration of the –COO– group, which indicated the formation of carboxylic groups (EDTA and DTPA) on the surface of the Fe_3O_4@SiO_2-AP.[59] As a result of the presence of large quantities of metallic Pt on the surface of the nanoparticles, the decrease in vibration of C=O and C–O suggests that the carboxyl group on the surface of the functional magnetic silica have coordinated with platinum, signifying the immobilization of platinum complex on the Fe_3O_4@SiO_2-EDTA and Fe_3O_4@SiO_2-DTPA surface.

XPS was used to further characterize the above catalysts (Fig. 5.). XPS results showed distinct Fe, O, N, C, Si and Pt peaks from the two novel nanoparticles (Fig. 5a). The detail XPS data for Fe_3O_4@SiO_2-AP, Fe_3O_4@SiO_2-EDTA@Pt, Fe_3O_4@SiO_2-DTPA@Pt and $H_2PtCl_6 \cdot 6H_2O$ were listed in Table 1. It revealed that the binding energies of Si 2p and O 1s in Fe_3O_4@SiO_2-EDTA@Pt and Fe_3O_4@SiO_2-DTPA@Pt were similar to those of Fe_3O_4@SiO_2-AP. The banding energy of Cl 2p in Fe_3O_4@SiO_2-EDTA@Pt and Fe_3O_4@SiO_2-DTPA@Pt was similar to that of $H_2PtCl_6 \cdot 6H_2O$. It was noteworthy that the banding energy of Pt 4f7/2 in Fe_3O_4@SiO_2-EDTA@Pt and Fe_3O_4@SiO_2-DTPA@Pt was 3–5 eV more than that in $H_2PtCl_6 \cdot 6H_2O$. It could be summarized that electron donation from carboxyl group to Pt to form the coordination bond between carboxyl and Pt in Fe_3O_4@SiO_2-EDTA@Pt and Fe_3O_4@SiO_2-DTPA@Pt, which was also consistent with the FT-IR results. The Pt 4f XPS spectra contain two peaks corresponding to Pt 4f7/2 and 4f5/2 states from the spin-orbital splitting and each peak was de-convoluted with Pt(0), Pt(II) and Pt(IV).[60–62] In Fe_3O_4@SiO_2-EDTA@Pt, the percentage of Pt^{4+}, Pt^{2+} and Pt^0 peaks were 28.9, 46.5 and 24.6%, respectively. In Fe_3O_4@SiO_2-DTPA@Pt, the ratio of Pt^{2+} (50.3%) and Pt^0 (26.4%) were higher than that of Fe_3O_4@SiO_2-EDTA@Pt, whereas the Pt^{4+} decreased to 23.3%. Results indicated the Pt^{2+} and Pt^0 were predominant species that may be corresponding to

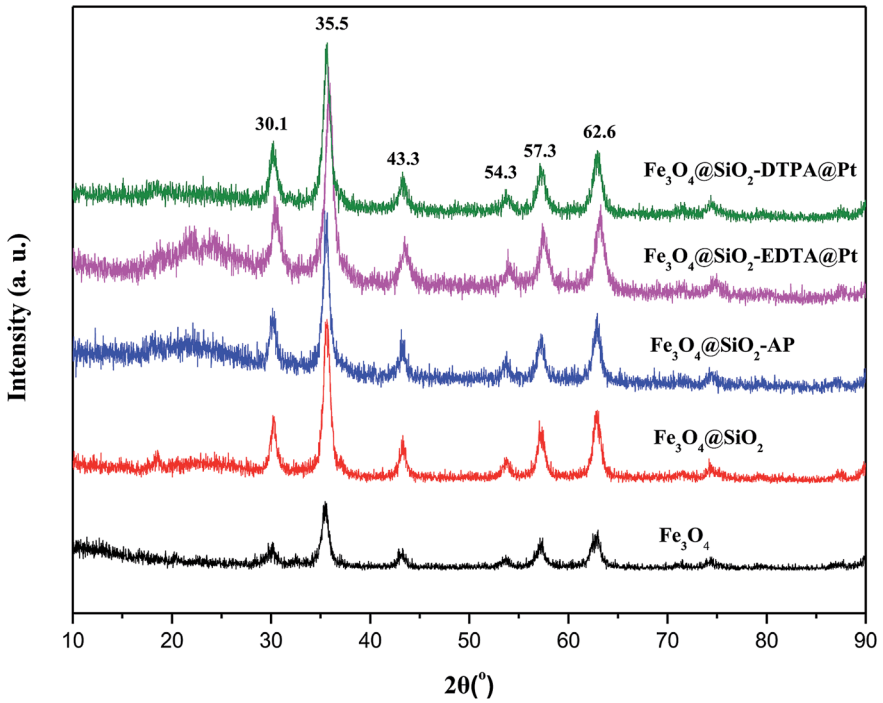

Fig. 3 XRD patterns of Fe_3O_4, Fe_3O_4@SiO_2, Fe_3O_4@SiO_2-AP, Fe_3O_4@SiO_2-EDTA@Pt and Fe_3O_4@SiO_2-DTPA@Pt nanoparticles.

good catalytic activity and might be produced on the catalyst surface through passivation process during the sample preparation.

BET analysis showed another important characteristic of the Pt catalysts. Fig. 6a shows the nitrogen adsorption isotherms and pore-size distribution of Fe_3O_4@SiO_2-EDTA@Pt and Fe_3O_4@SiO_2-DTPA@Pt catalysts. Both of two samples showed type III isotherms with type H3 hysteresis loops which is related to the slit-like pores because of aggregation of particles.[63] When we dispersed these nanoparticles in aqueous solution and

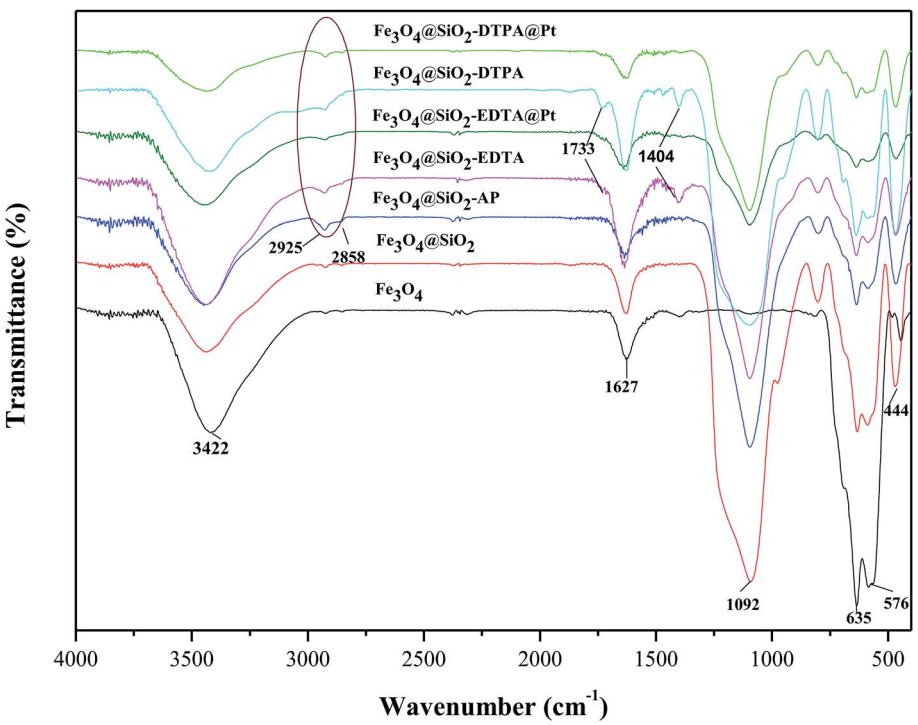

Fig. 4 FT-IR spectra of Fe_3O_4, Fe_3O_4@SiO_2, Fe_3O_4@SiO_2-AP, Fe_3O_4@SiO_2-EDTA, Fe_3O_4@SiO_2-EDTA@Pt, Fe_3O_4@SiO_2-DTPA, and Fe_3O_4@SiO_2-DTPA@Pt nanoparticles.

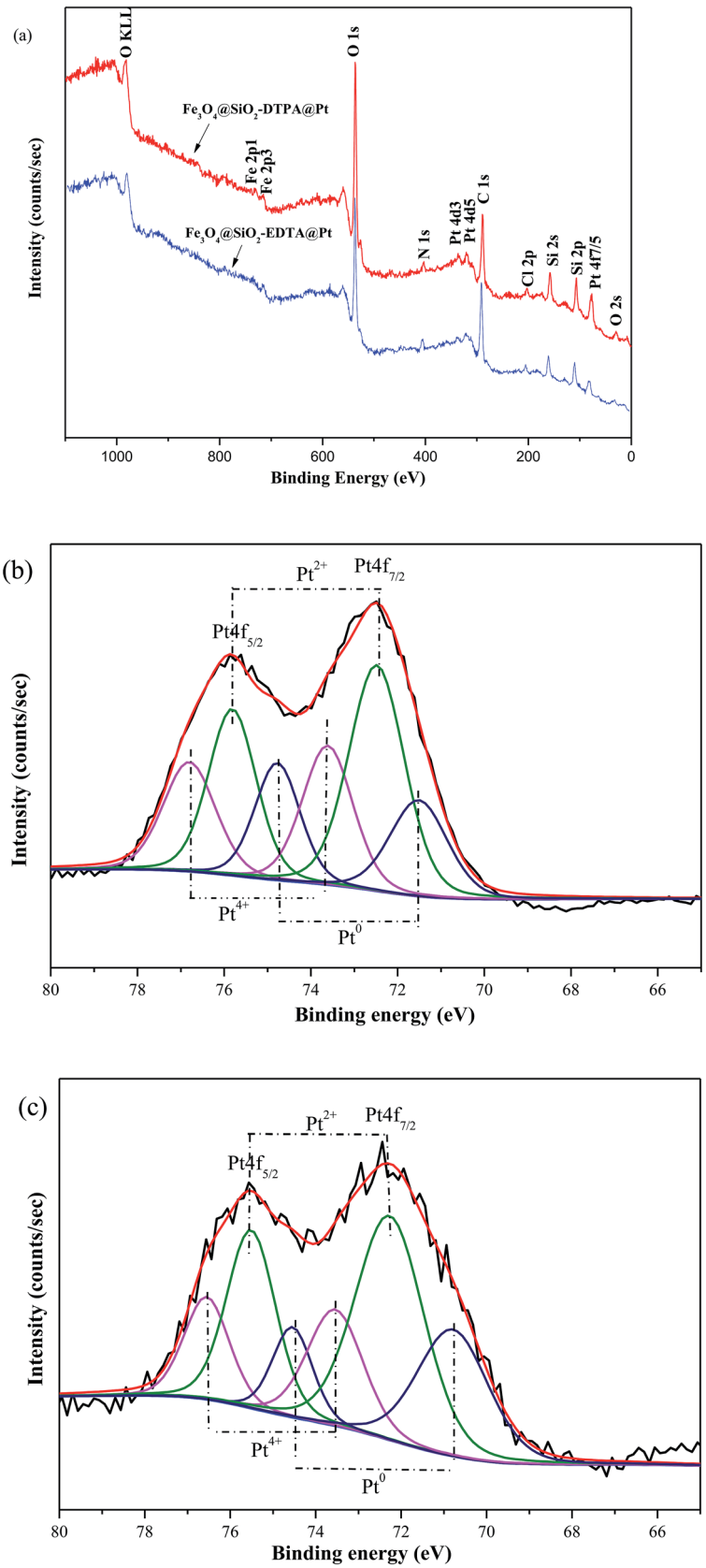

Fig. 5 (a) XPS spectra of Fe_3O_4@SiO_2-EDTA@Pt and Fe_3O_4@SiO_2-DTPA@Pt. (b) High-resolution XPS spectra of Pt 4f for Fe_3O_4@SiO_2-EDTA@Pt. (c) High-resolution XPS spectra of Pt 4f for Fe_3O_4@SiO_2-DTPA@Pt.

Table 1 XPS data for Fe_3O_4@SiO_2-EDTA@Pt and Fe_3O_4@SiO_2-DTPA@Pt, Fe_3O_4@SiO_2-AP and $H_2PtCl_6 \cdot 6H_2O$ (eV)[a]

Samples	Pt 4f7/2	Si 2p	N 1s	O 1s	Cl 2p
Fe_3O_4@SiO_2-EDTA@Pt	78.40	107.21	405.59	536.88	201.29
Fe_3O_4@SiO_2-DTPA@Pt	76.80	106.40	403.23	536.86	200.40
Fe_3O_4@SiO_2-AP	—	108.78	407.24	537.60	—
$H_2PtCl_6 \cdot 6H_2O$	73.10	—	—	—	199.50

[a] The banding energies are referred to C 1s (284.6 eV).

observed using microscope, these nanoparticles were monodisperse. It means the aggregation is temporary in BET analysis. The BET data including surface area, average pore size and total pore volume derived from the isotherms were calculated. The BET specific surface area, the pore size and the total pore volume of Fe_3O_4@SiO_2-EDTA@Pt were 75.68 $m^2\ g^{-1}$, 17.50 nm and 0.685 $cm^3\ g^{-1}$, respectively. They were corresponding to 36.65 $m^2\ g^{-1}$, 29.86 nm and 0.366 $cm^3\ g^{-1}$ for Fe_3O_4@SiO_2-DTPA@Pt.

To test the thermal stability and the grafting amount of carboxyl groups on the magnetic silica nanoparticles, TGA analysis was performed for Fe_3O_4@SiO_2-EDTA@Pt and Fe_3O_4@SiO_2-DTPA@Pt nanoparticles (Fig. 6b.). As shown in the TGA curve of the prepared nanoparticles, the weight loss below 200 °C was attributed to the removal the water, and the organic parts were decomposed completely at about 700 °C. The TGA curve of bare Fe_3O_4@SiO_2 nanoparticles showed that the weight loss over a temperature range from 50 to 800 °C was about 4%, which was attributed to the escape of physically adsorbed water or/and structural water on the surface.[64] Moreover, the weight increases slightly in the temperature range of 700–800 °C, which might be caused by the slight oxidation of Fe_3O_4.[65] For Fe_3O_4@SiO_2-EDTA@Pt and Fe_3O_4@SiO_2-DTPA@Pt nanoparticles, the weight loss at temperatures below 200 °C was about 3%, which was related to the release of moisture and structural water on the surface of the silica layer. However, apart from the water loss, organic components inside the particles began to degrade rapidly at a temperature higher than 200 °C, and almost completely decomposed at 550 °C for Fe_3O_4@SiO_2-EDTA@Pt and 700 °C for Fe_3O_4@SiO_2-DTPA@Pt, respectively. Therefore, the weight loss from 200 to 800 °C in the TGA curves of Fe_3O_4@SiO_2-EDTA@Pt (about 28 wt%) and Fe_3O_4@SiO_2-DTPA@Pt (about 30 wt%) could be used to estimate the weight proportions of EDTA or DTPA-modified on Fe_3O_4@SiO_2. This phenomenon suggested that the weight proportion of multi-carboxyl groups on Fe_3O_4@SiO_2-DTPA@Pt (30 wt%) was higher than that on Fe_3O_4@SiO_2-EDTA@Pt (28 wt%). It was consistent with one more carboxyl group in DTPA than EDTA.

The key for magnetic materials is the sufficient magnetic property. Therefore the magnetic properties of these nanoparticles were analyzed by VSM (Fig. 7.). The saturation magnetization was found to be 74.7, 48.4, 44.4, 25.4 and 23.0 emu g^{-1} for Fe_3O_4, Fe_3O_4@SiO_2, Fe_3O_4@SiO_2-AP, Fe_3O_4@SiO_2-EDTA@Pt and Fe_3O_4@SiO_2-DTPA@Pt, respectively. All of them showed superparamagnetic properties due to the presence of nanometer-sized magnetic Fe_3O_4 particles in the core.[66] Although the saturation magnetization values of Fe_3O_4@SiO_2-EDTA@Pt and Fe_3O_4@SiO_2-DTPA@Pt were lower than that of Fe_3O_4, Fe_3O_4@SiO_2 and Fe_3O_4@SiO_2-AP, they could be readily separated from their dispersion in 1 min with an external magnetic field owing to their high magnetite content and thus good magnetic response (Fig. 7, inset). These results indicated that the magnetization of Fe_3O_4 decreases considerably after coated with SiO_2 due to the weight contribution from the nonmagnetic SiO_2. Nevertheless, both of the catalysts exhibited enough magnetic response to meet the need of magnetic separation.

3.3. Catalyst performances for hydrosilylation

3.3.1 Activity and reusability in catalyzing hydrosilylation of 1-hexene. Hydrosilylation of alkene with silane is a typical reaction catalyzed by platinum, which exist two reaction pathways α-addition and β-addition.[67,68] Hydrosilylation of a series of alkenes with methyldichlorosilane were catalyzed by the two novel Pt catalysts, Fe_3O_4@SiO_2-EDTA@Pt and Fe_3O_4@SiO_2-DTPA@Pt, to evaluate their activity and regioselectivity.

Hydrosilylation conditions are important for yield and regioselectivity. To exhibit well the activities of two catalysts, we optimized hydrosilylation conditions of 1-hexene and methyldichlorosilane, including reaction temperatures (30, 40, 50, 60, 70, and 80 °C), times (0.5, 1, 2, 3, 4, and 5 h), the molar ratio of methyldichlorosilane and 1-hexene (0.5 : 1.0, 1.0 : 1.0, 1.2 : 1.0, 1.5 : 1.0, 1.8 : 1.0, and 2.0 : 1.0) and the additive sequence of 1-hexene and methyldichlorosilane (1-hexene added to methyldichlorosilane after methyldichlorosilane mixing with the catalyst for 30 min, simultaneous addition of 1-hexene and methyldichlorosilane, methyldichlorosilane added to 1-hexene after mixing with the catalyst for 30 min). The detail results were summarized in support information (Fig. 1S†). Results indicated both Fe_3O_4@SiO_2-EDTA@Pt and Fe_3O_4@SiO_2-DTPA@Pt (containing 2.01 × 10^{-3} mmol Pt in each catalyst) could efficiently catalyze the hydrosilylation. The yields were up to 99.4% and 98.77% when 19.2 mmol methyldichlorosilane was added to 11.8 mmol 1-hexene after mixing with the catalyst for 30 min and maintained the reaction 3 h at 50–60 °C. As a comparison, the yield only was 35.46% when Fe_3O_4@SiO_2@Pt was used as catalyst.

In research of platinum catalyst, the turnover number (TON) of Pt often is used as criteria. Thus, we calculated the TON approached 3628 and 3550 when Fe_3O_4@SiO_2-EDTA@Pt and Fe_3O_4@SiO_2-DTPA@Pt with 2.60 μmol Pt catalyzed 11.2 mmol of 1-hexene in 4 h. To further increase the TON for hydrosilylation, amount of Pt catalyst was gradually decreased to 2.10, 1.82, 1.47, 0.87, even 0.34 μmol. Results indicated the hydrosilylation between 1-hexene and methyldichlorosilane with low amount of Pt could be catalyzed and the TON quickly increased to 4721, 5435, 6744, 10 905 and 16 006 for Fe_3O_4@SiO_2-EDTA@Pt, 4750, 5464, 6794 and 10 789 for Fe_3O_4@SiO_2-DTPA@Pt. Furthermore, we catalyzed the hydrosilylation of methyldichlorosilane (180 mmol) and 1-hexene (110 mmol) using only 0.3 mg Fe_3O_4@SiO_2-EDTA@Pt (0.0052 μmol Pt) or 0.3 mg Fe_3O_4@SiO_2-DTPA@Pt (0.057 μmol Pt) in 12 h.

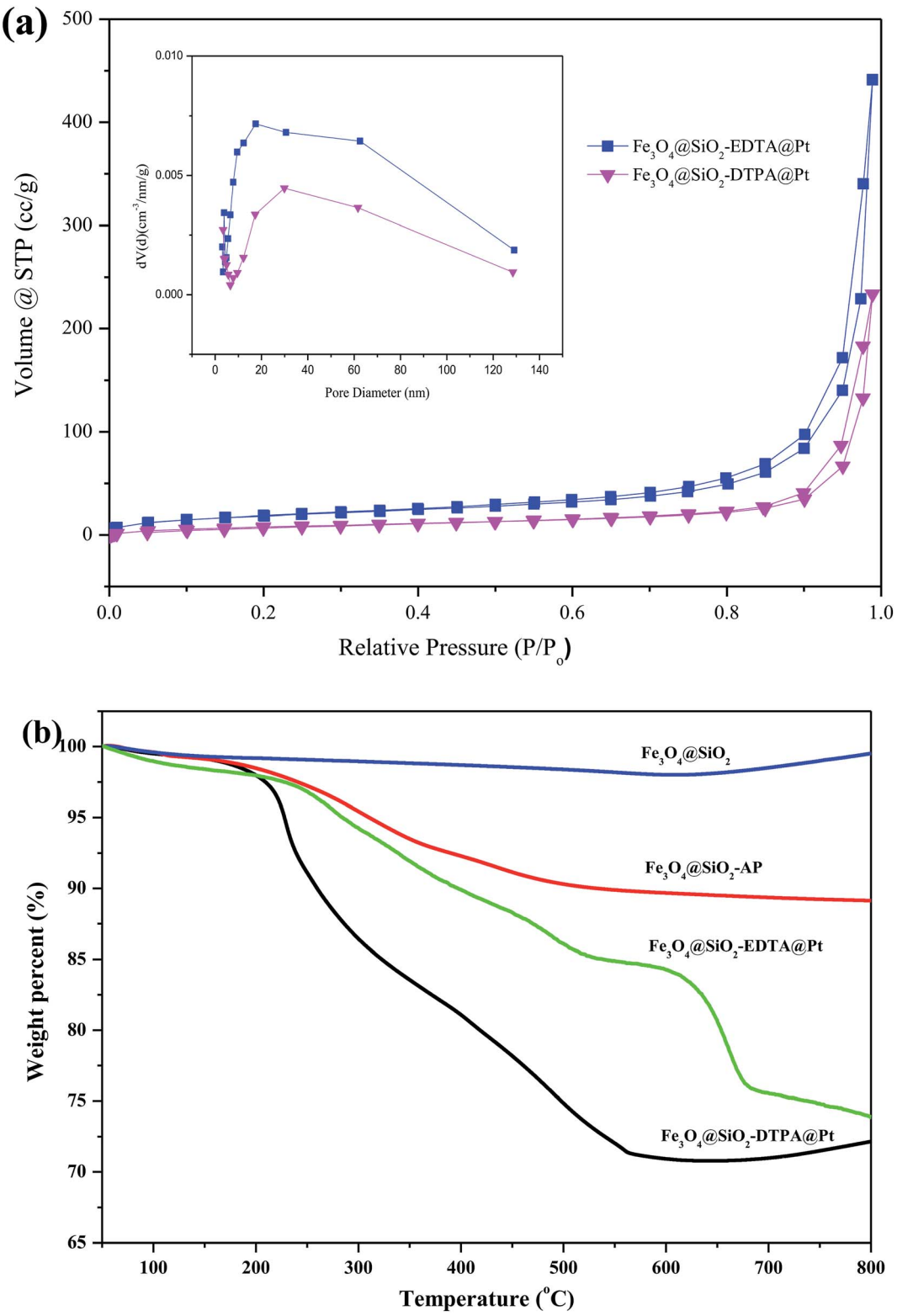

Fig. 6 (a) Nitrogen adsorption–desorption isotherms and (inset) the corresponding pore-size distribution curves of Fe_3O_4@SiO_2, Fe_3O_4@SiO_2-AP, Fe_3O_4@SiO_2-EDTA@Pt and Fe_3O_4@SiO_2-DTPA@Pt catalysts, (b) TGA curves of Fe_3O_4@SiO_2, Fe_3O_4@SiO_2-AP, SiO_2@Fe_3O_4-EDTA@Pt and SiO_2@Fe_3O_4-DTPA@Pt.

Remarkably, the region-selectivity was still around 99% and TON increased to 662 733 for Fe_3O_4@SiO_2-EDTA@Pt, 579 947 for Fe_3O_4@SiO_2-DTPA@Pt, respectively.

Usually, the stability of a catalyst is an important characteristic before it can be used in an industrial application. Therefore, the reusability of Fe_3O_4@SiO_2-EDTA@Pt and

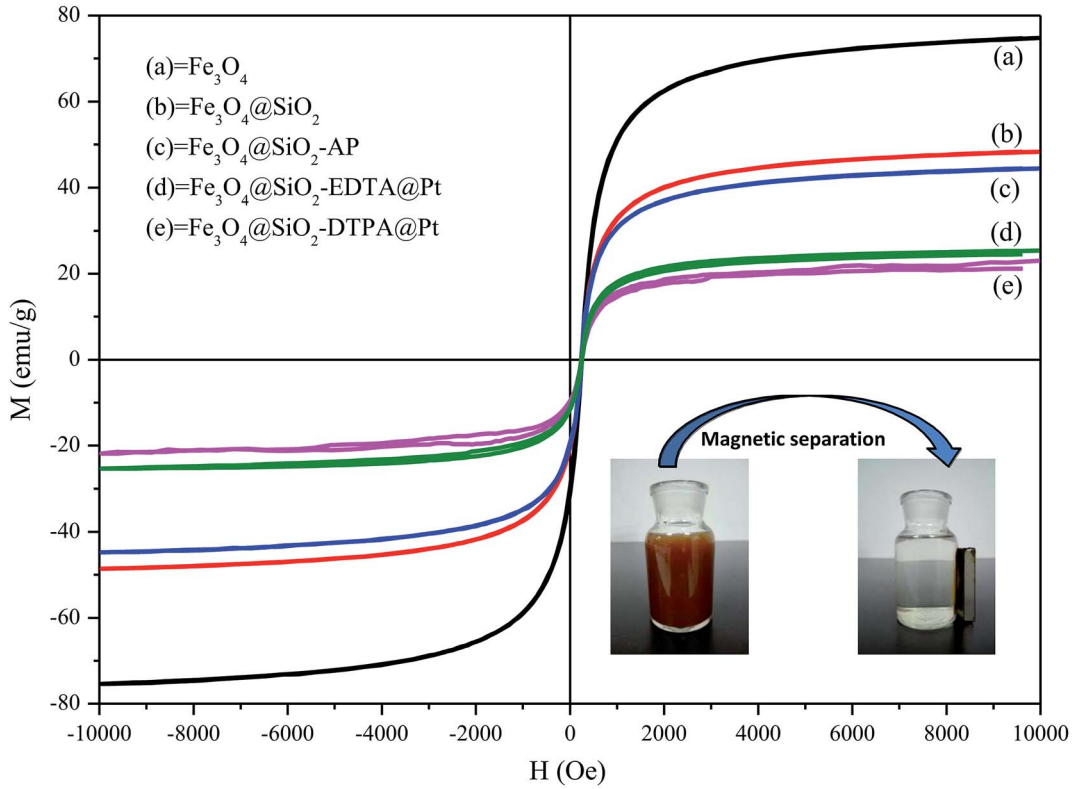

Fig. 7 VSM magnetization curves of Fe_3O_4, Fe_3O_4@SiO_2, Fe_3O_4@SiO_2-AP, Fe_3O_4@SiO_2-EDTA@Pt and Fe_3O_4@SiO_2-DTPA@Pt. Inset: magnetic separation of Fe_3O_4@SiO_2-EDTA@Pt and Fe_3O_4@SiO_2-DTPA@Pt from the aqueous suspensions.

Fe_3O_4@SiO_2-DTPA@Pt catalysts were evaluated through repetitively catalyzing the hydrosilylation of 1-hexene with methyldichlorosilane. A series of 12 consecutive hydrosilylation reactions were carried out under optimal reaction conditions. After each catalytic reaction, the two platinum catalysts were held in the original system using a magnet and catalyzed next hydrosilylation without any other process. The results were showed in Fig. 8. Data showed a satisfactory yield of 1-heptylmethyldichlorosilane (about 90% after 12 catalytic runs for both of Pt catalysts) which was apparent better than the Pt catalysts immobilized on non-magnetic SiO_2 supports (only 80% after 12 or 13 runs).[36,37] After 12 runs, the magnetism both of Pt catalysts were similar and the platinum amount was 155.78 mmol g^{-1} for Fe_3O_4@SiO_2-EDTA@Pt and 177.62 mmol g^{-1} for Fe_3O_4@SiO_2-DTPA@Pt. There were only 10.4% Pt loss in Fe_3O_4@SiO_2-EDTA@Pt and 7.9% Pt loss in Fe_3O_4@SiO_2-DTPA@Pt. The average loss of Pt was 0.87% for Fe_3O_4@SiO_2-EDTA@Pt and 0.66% for Fe_3O_4@SiO_2-DTPA@Pt in each reaction which was apparent better than homogeneous Pt catalyst (about 10 ppm) and Pt catalysts immobilized on non-magnetic support. The data were listed in Table S1.† In order to identify the active species of Pt catalysts, the state of Pt catalysts in high-resolution XPS after recycle experiments was tested. The data were listed in Fig. S3 and Table S2.† The total amount of Pt^{2+} and Pt^0 was 71.1% (before recycle) and 76.1% (after recycle) for Fe_3O_4@SiO_2-EDTA@Pt. The total amount of Pt^{2+} and Pt^0 was 73.6% (before recycle) and 79.6% (after recycle) for Fe_3O_4@SiO_2-DTPA@Pt. According to the data, there wasn't the apparent state change of the recycled Pt catalyst in both Fe_3O_4@SiO_2-EDTA@Pt and Fe_3O_4@SiO_2-DTPA@Pt. This also indicated both of catalysts, especially Fe_3O_4@SiO_2-DTPA@Pt, were very stable, which maybe result from strong coordination interaction between carboxyl group and the metallic Pt. The residual four carboxyl groups of DTPA in Fe_3O_4@SiO_2-DTPA maybe produce a stronger interaction with Pt than the residual three carboxyl groups of EDTA in Fe_3O_4@SiO_2-EDTA (Table 2).

3.3.2 Catalyzing hydrosilylation of internal and terminal hexene. The unprecedented activity and selectivity of the two Pt nanoparticle catalysts prompted us to further exploit its potential applications in the isomerization–hydrosilylation tandem process. Five hexene, including 1-hexene, *trans*-2-hexene, *cis*-2-hexene, *trans*-3-hexene and *cis*-3-hexene were used as alkene. The hydrosilylation between methyldichlorosilane and hexene were catalyzed by Fe_3O_4@SiO_2-EDTA@Pt or Fe_3O_4@SiO_2-DTPA@Pt under the aforementioned optimal conditions. Products were monitored by GC and NMR (see Fig. S2 in ESI†). Data were summarized in Table 3. It was interesting that the main product was 1-hexylmethyldichlorosilane in hydrosilylation of all of hexene, which was typical isomerization–hydrosilylation and the β-adduct as a major product. The similar phenomena were observed in previous studies.[69,70] We bought the standard substance of 1-hexylmethyldichlorosilane which was compared with the synthesized 1-hexylmethyldichlorosilane, in GC chromatograms, all 1-

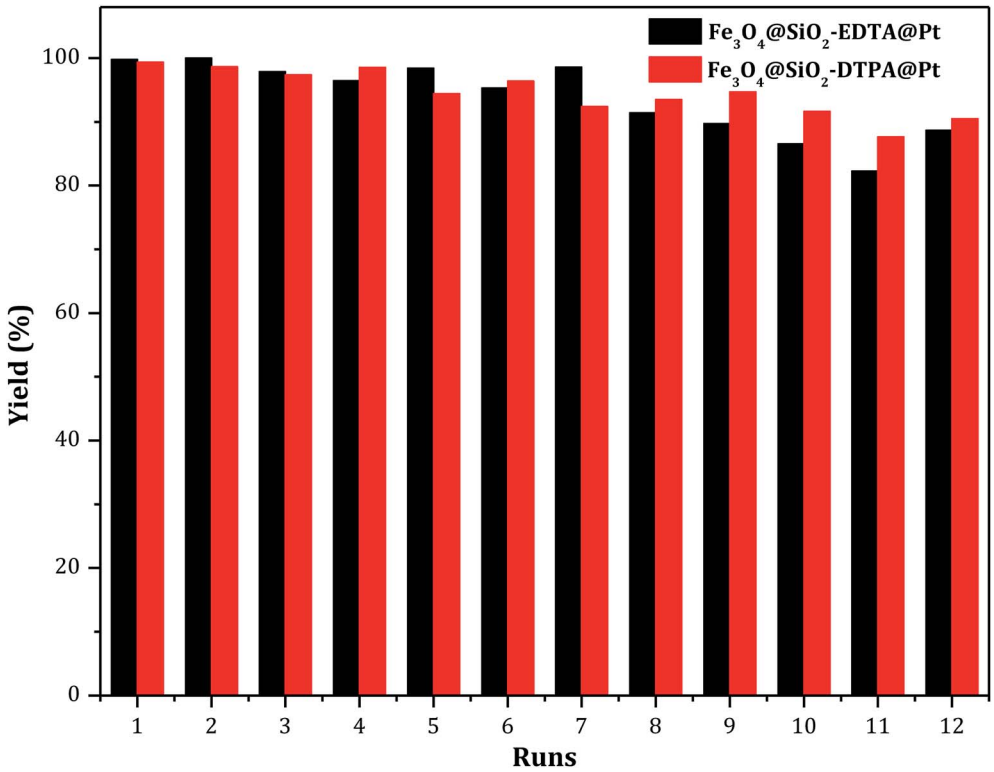

Fig. 8 Catalyst recycle experiments for the hydrosilylation of 1-hexene with methyldichlorosilane.

hexylmethyldichlorosilane peek shown at around 8.45 min. For NMR: ^{1}H NMR (600 MHz, $CDCl_3$) δ: 1.50 (m, 2H, CH_3–$(CH_2)_3$–CH_2–CH_2–$SiCl_2$–CH_3), 1.38 (m, 2H, CH_3–$(CH_2)_2$–CH_2–$(CH_2)_2$–$SiCl_2$–CH_3), 1.20 (s, 4H, CH_3–$(CH_2)_2$–$(CH_2)_3$–$SiCl_2$–CH_3), 1.12 (m, 2H, CH_3–$(CH_2)_4$–CH_2–$SiCl_2$–CH_3), 0.88 (t, 3H, CH_3–$(CH_2)_5$–$SiCl_2$–CH_3), 0.77 (s, 3H, CH_3–$(CH_2)_5$–$SiCl_2$–CH_3).

The yield of 1-hexylmethyldichlorosilane changed in hydrosilylation of different hexane and methyldichlorosilane. When Fe_3O_4@SiO_2-EDTA@Pt was used as catalyst, the highest yield (97%) was from 1-hexene. The yield of 1-hexylmethyldichlorosilane decreased to 95% for *cis*-2-hexene and 83% for *cis*-3-hexene. When *cis*-2-hexene and *cis*-3-hexene were changed to

Table 2 Fe_3O_4@SiO_2-EDTA@Pt and Fe_3O_4@SiO_2-DTPA@Pt-catalyzed tandem isomerization–hydrosilylation of *trans*- and *cis*-internal alkenes with methyldichlorosilane[a]

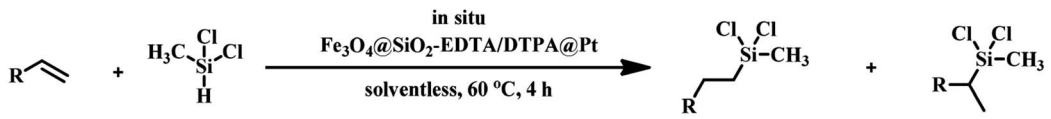

Alkene Methyldichlorosilane β -adduct α -adduct

		Yield[b] (%)			β/α	
Entry	Alkene	*a*	*b*	Product	*a*	*b*
1		97	99		>20 : 1	>20 : 1
2		87	88		>20 : 1	>20 : 1
3		95	98	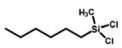	>20 : 1	>20 : 1
4		78	84		>20 : 1	>20 : 1
5		83	87		>20 : 1	>20 : 1

[a] Conditions: alkenes, 10 mmol; methyldichlorosilane, 15 mmol; 8 h; a, Fe_3O_4@SiO_2-EDTA@Pt as catalyst; b Fe_3O_4@SiO_2-DTPA@Pt as catalyst. [b] yield were determined by GC using *n*-decane as an internal standard.

Table 3 Hydrosilylation of alkenes with methyldichlorosilane catalyzed by Fe_3O_4@SiO_2-EDTA@Pt and Fe_3O_4@SiO_2-DTPA@Pt[a]

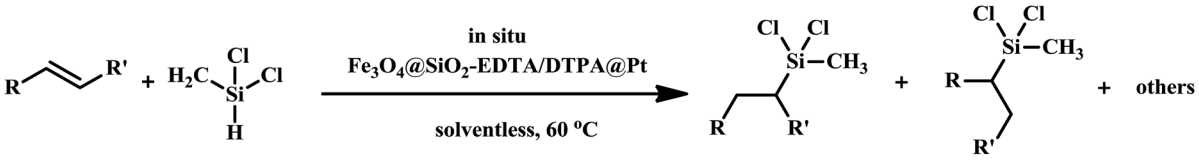

Entry	Alkene	Structure	Time/h	Conv.[b] (%) a	Conv.[b] (%) b	TOF[c] (10^3 h^{-1}) a	TOF[c] (10^3 h^{-1}) b
1	Cyclohexene		4	2	13	<0.1	<0.1
2	*N*,*N*-Dimethylacrylamide		4	96	98	8.9	8.2
3	1,2-Epoxy-4-vinylcyclohexane		4	99	98	9.5	9.3
4	Norbornylene		4	97	99	7.1	6.8
5	Methyl methacrylate		5	58	67	4.9	5.1
6	Butyl acrylate	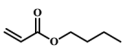	5	57	87	4.1	3.8
7	Ethane-1,2-diyl bis(2-methylacrylate)	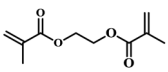	5	72	81	5.1	5.8
8	Crotonic acid ethyl ester	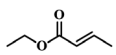	5	69	87	6.6	6.1
9	*trans*-2-Hexenyl acetate	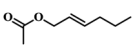	5	68	97	5.6	4.9
10	*trans*-2-Hexen-1-yl phenylacetate	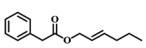	6	61	68	7.0	8.2
11	1,2-Epoxy-7-octene	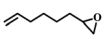	6	98	99	8.7	9.1
12	Allyl glycidyl ether		6	84	98	5.1	4.4
13	5-Hexen-2-one		6	86	97	8.2	7.6
14	Allylchloride		4	58	64	6.2	6.1

[a] Conditions: 15 mmol methyldichlorosilane, 10 mmol alkene; temperature: 60 °C; a, Fe_3O_4@SiO_2-EDTA@Pt as catalyst (1.74×10^{-3} mmol Pt); b, Fe_3O_4@SiO_2-DTPA@Pt as catalyst (1.93×10^{-3} mmol Pt). [b] The conversion was based on the amount of alkene consumed. [c] Initial TOFs were calculated by GC after 30 min of reaction time.

trans-2-hexene and *trans*-3-hexene, the yield further decreased corresponding to 87% and 78%. The similar phenomenon was observed when Fe_3O_4@SiO_2-DTPA@Pt was used as catalyst. It indicated the hydrosilylation was harder for internal hexane than 1-hexene and *trans*-hexene than *cis*-hexane. The results also verified both of Pt catalysts could be used for the remote functionalization of alkenes, which has been shown to be a remarkable step in organic synthesis.[71,72]

3.3.3 Catalyzing hydrosilylation of other alkenes. The catalytic activities of the two Pt nanoparticles were further evaluated through employing another 14 alkenes with different substituent, including nine terminal alkenes (*N*,*N*-dimethylacrylamide, 1,2-epoxy-4-vinylcyclohexane, methyl methacrylate, butyl acrylate, ethane-1,2-diyl bis(2-methylacrylate), 1,2-epoxy-7-octene, allyl glycidyl ether, 5-hexen-2-one and allylchloride), three *trans*- internal alkenes (crotonic acid ethyl ester, *trans*-2-hexenyl acetate, and *trans*-2-hexen-1-yl phenylacetate) and two ring type alkenes (cyclohexene and norbornylene). These compounds are important industry raw materials. For example, allyl glycidyl ether is an important substrate because the alkoxysilanes derived from this alkene have broad applications in coatings and as coupling agents for epoxy composites used as electronic chip encapsulation.[73] Catalytic results were summarized in Table 3. The multi-products were observed in GC chromatograms, different substrates peak at different times due to the diversity of their boiling point, for example, cyclohexene peek at around 6.86 min, 1,2-epoxy-4-vinylcyclohexane peek at around 9.55 min, and allyl glycidyl ether peek at around

8.18 min. Because of multi-products were observed, *n*-decane used as internal standard to get alkene conversion, which used to evaluate the versatility of the prepared catalysts. Various linear alkenes containing either electron-donating or electron-withdrawing groups such as amine (entry 2), ester (entries 5–10), epoxide (entries 3, 11, and 12), ketone (entry 13), alkyl chloride (entry 14) and ring type norbornylene (entry 4) except cyclohexene (entry 1) were well catalyzed by Fe_3O_4@SiO_2-EDTA@Pt and Fe_3O_4@SiO_2-DTPA@Pt. In catalyzing *N*,*N*-dimethylacrylamide, 1,2-epoxy-4-vinylcyclohexane, norbornylene, and 1,2-epoxy-7-octene, both Fe_3O_4@SiO_2-EDTA@Pt and Fe_3O_4@SiO_2-DTPA@Pt showed similar high activity (>96%). The catalytic activity of Fe_3O_4@SiO_2-DTPA@Pt was significantly higher than Fe_3O_4@SiO_2-EDTA@Pt in hydrosilylation of crotonic acid ethyl ester, *trans*-2-hexen-1-yl phenylacetate, *trans*-2-hexenyl acetate, methyl methacrylate, butyl acrylate, ethane-1,2-diyl bis(2-methylacrylate), allyl glycidyl ether, 5-hexen-2-one and allylchloride. Even Fe_3O_4@SiO_2-DTPA@Pt could catalyze the hydrosilylation of cyclohexene (13%), whereas a very low yield (2%) in Fe_3O_4@SiO_2-EDTA@Pt as catalyst. These results indicated Fe_3O_4@SiO_2-EDTA@Pt was more efficient.

4. Conclusions

Two novel magnetic Fe_3O_4@SiO_2-EDTA@Pt and Fe_3O_4@SiO_2-DTPA@Pt catalysts were successfully prepared. The saturation magnetization was 25.4 and 23.0 emu g^{-1} for Fe_3O_4@SiO_2-EDTA@Pt and Fe_3O_4@SiO_2-DTPA@Pt, respectively. The Pt amount of the 30–50 nm nanoparticles was corresponding to 173.80 and 192.77 μmol g^{-1}, which the predominant valence was Pt^{2+} and Pt^0. In catalyzing hydrosilylation of 1-hexene and methyldichlorosilane, the yield of 1-heptylmethyldichlorosilane was about 99% for both of catalysts and the TON were up to 662 733 for Fe_3O_4@SiO_2-EDTA@Pt and 579 947 for Fe_3O_4@SiO_2-DTPA@Pt, respectively. The two catalysts, especially Fe_3O_4@SiO_2-DTPA@Pt, showed good activity in hydrosilylation of 5 isomerous hexanes and 14 other alkene with different substituent. Fe_3O_4@SiO_2-DTPA@Pt even could catalyze the hydrosilylation of cyclohexene. After 12 catalytic runs for both of Pt catalysts, yield of 1-heptylmethyldichlorosilane was still up to 90% and the magnetism was similar. The average loss of Pt in each reaction was 0.87% for Fe_3O_4@SiO_2-EDTA@Pt and 0.66% for Fe_3O_4@SiO_2-DTPA@Pt. The unprecedented activity and selectivity of the two Pt nanoparticle catalysts are prospective and potential in catalyzing more reactions and replacing the current homogeneous Pt catalyst industry.

Conflicts of interest

There are no conflicts to declare.

Acknowledgements

The authors would like to appreciate the financial supports from the National Natural Science foundation of China (No. 21605112).

References

1 R. M. Cornell and U. Schwertmann, *The Iron Oxides: Structure, Properties, Reactions, Occurrence and Uses*, VCH Publications, Weinheim, New York, 1996.
2 S. Xuan, Y. X. Wang, J. C. Yu and K. C. Leung, *Langmuir*, 2009, **25**, 11835–11843.
3 B. Gaihre, M. S. Khil, D. R. Lee and H. Y. Kim, *Int. J. Pharm.*, 2009, **365**, 180–189.
4 N. Kohler, C. Sun, A. Fichtenholtz, J. Gunn, C. Fang and M. Zhang, *Small*, 2006, **2**, 785–792.
5 H. Lee, M. K. Yu, S. Park, S. Moon, J. J. Min, Y. Y. Jeong, H. W. Kang and S. Jon, *J. Am. Chem. Soc.*, 2007, **129**, 12739–12745.
6 H. Liu, Z. Jia, S. Ji, Y. Zheng, M. Li and H. Yang, *Catal. Today*, 2011, **175**, 293–298.
7 A. M. Donia, A. A. Atia and K. Z. Elwakeel, *J. Hazard. Mater.*, 2008, **151**, 372–379.
8 N. Nuryono, N. M. Rosiati, B. Rusdiarso, S. C. W. Sakti and S. Tanaka, *SpringerPlus*, 2014, **3**, 515–526.
9 S. Hokkanen, E. Repo, S. Lou and M. Sillanpaa, *Chem. Eng. J.*, 2015, **260**, 886–894.
10 X. Sun, Q. Li, L. Yang and H. Liu, *Particuology*, 2016, **26**, 79–86.
11 A. Khazaei, M. Khazaei and M. Nasrollahzadeh, *Tetrahedron*, 2017, **73**, 5624–5633.
12 Y. Fang, Y. Chen, X. Li, X. Zhou, J. Li, W. Tang, J. Huang, J. Jin and J. Ma, *J. Mol. Catal. A: Chem.*, 2014, **392**, 16–21.
13 B. Panella, A. Vargas and A. Baiker, *J. Catal.*, 2009, **261**, 88–93.
14 R. L. Oliveira, P. K. Kiyohara and L. M. Rossi, *Green Chem.*, 2010, **12**, 144–149.
15 M. Amir, U. Kurtan and A. Baykal, *Chin. J. Catal.*, 2015, **36**, 1280–1286.
16 J. Sun, Z. Dong, X. Sun, P. Li, F. Zhang, W. Hu, H. Yang, H. Wang and R. Li, *J. Mol. Catal. A: Chem.*, 2013, **367**, 46–51.
17 J. J. Martíneza, E. X. Aguileraa, J. Cubillosa, H. Rojasa, A. Gómez-Cortésb and G. Díaz, *Mol. Catal.*, 2019, **465**, 54–60.
18 S. A. Theofanidis, V. V. Galvita, H. Poelman, R. Batchu, L. C. Buelens, C. Detavernier and G. B. Marin, *J. Mol. Catal. B: Enzym.*, 2018, **239**, 502–512.
19 Z. Mohamed, V. D. Dasireddy, S. Singh and H. B. Friedrich, *Int. J. Hydrogen Energy*, 2018, **43**, 22291–22302.
20 B. Cheng, W. Liu and Z. Lu, *J. Am. Chem. Soc.*, 2018, **140**, 5014–5017.
21 B. Panella, A. Vargas and A. Baiker, *J. Catal.*, 2009, **261**, 88–93.
22 M. Walczak, K. Stefanowska, A. Franczyk, J. Walkowiak, A. Wawrzynczak and B. Marciniec, *J. Catal.*, 2018, **367**, 1–6.
23 T. Yang, Y. Huo, Y. Liu, Z. Rui and H. Ji, *Appl. Catal., B*, 2017, **200**, 543–551.
24 H. A. Khan, P. Natarajan and K. Jung, *Appl. Catal., B*, 2018, **231**, 151–160.
25 H. Zai, Y. Zhao, S. Chen, L. Ge and C. Chen, *Nano Res.*, 2018, **61**, 2544–2552.

26 Q. Li, S. Ji, M. Li and X. Duan, *Sci. China Mater.*, 2018, **11**, 1339–1344.
27 M. Mahmoudi, S. Sant, B. Wang, S. Laurent and T. Sen, *Adv. Drug Delivery Rev.*, 2011, **63**, 24–46.
28 R. T. Yang, *Adsorbents: Fundamentals and Applications*, John Wiley & Sons, USA, 2003.
29 A. Lu, E. L. Salabas and F. Schüth, *Angew. Chem., Int. Ed.*, 2007, **46**, 1222–1244.
30 G. Zeng, Y. Pang, Z. Zeng, L. Tang, Y. Zhang, Y. Liu, J. Zhang, X. Lei, Z. Li, Y. Xiong and G. Xie, *Langmuir*, 2012, **28**, 468–473.
31 J. Ramo, M. Sillanpaa, V. Vickackaite, M. Orama and L. Niinisto, *J. Pulp Pap. Sci.*, 2000, **26**, 125–131.
32 J. Ramo and M. Sillanpaa, *J. Cleaner Prod.*, 2001, **9**, 191–195.
33 M. E. T. Sillanpaa and J. H. P. Ramo, *Environ. Sci. Technol.*, 2001, **35**, 1379–1384.
34 M. Sillanpaa, M. Orama, J. Ramo and A. Oikari, *Sci. Total Environ.*, 2001, **267**, 23–31.
35 K. Pirkanniemi, S. Metsarinne and M. Sillanpaa, *J. Hazard. Mater.*, 2007, **147**, 556–561.
36 F. Li and Y. Li, *J. Mol. Catal. A: Chem.*, 2016, **420**, 254–263.
37 D. Shao and Y. Li, *RSC Adv.*, 2018, **8**, 20379–20393.
38 Z. Lu, G. Wang, J. Zhuang and W. Yang, *Colloids Surf., A*, 2006, **278**, 140–143.
39 Y. S. Kang, S. Risbud, J. F. Rabolt and P. Stroeve, *Chem. Mater.*, 1996, **8**, 2209–2211.
40 S. Zhang, H. Niu, Y. Zhang, J. Liu, Y. Shi, X. Zhang and Y. Cai, *J. Chromatogr. A*, 2012, **1238**, 38–45.
41 Y. Deng, D. Qi, C. Deng, X. Zhang and D. Zhao, *J. Am. Chem. Soc.*, 2008, **130**, 28–29.
42 M. J. Jacinti, O. H. Santos, R. Landers, P. K. Kiyohara and L. M. Rossi, *Appl. Catal., B*, 2009, **90**, 688–692.
43 Z. Ma, Y. Guan and H. Liu, *J. Magn. Magn. Mater.*, 2006, **301**, 469–477.
44 Q. Yuan, N. Li, Y. Chi, W. Geng, W. Yan, Y. Zhao, X. Li and B. Dong, *J. Hazard. Mater.*, 2013, **254–255**, 157–165.
45 X. Sun, Q. Li, L. Yang and H. Liu, *Particuology*, 2016, **26**, 79–86.
46 M. J. Jacinto, P. K. Kiyohara, S. H. Masunaga, R. F. Jardim and L. M. Rossi, *Appl. Catal., A*, 2008, **338**, 52–57.
47 M. Tülü and K. E. Geckeler, *Polym. Int.*, 1999, **48**, 909–914.
48 Y. Liu, M. Chen and Y. Hao, *Chem. Eng. J.*, 2013, **218**, 46–54.
49 Y. Shiraishi, G. Nishimura, A. T. Hirai and I. Komasawa, *Ind. Eng. Chem. Res.*, 2002, **41**, 5065–5070.
50 E. Repoa, J. K. Warcholc, T. A. Kurniawana and M. E. T. Sillanpää, *Chem. Eng. J.*, 2010, **161**, 73–82.
51 M. A. Hughes and E. Rosenberg, *Sep. Sci. Technol.*, 2007, **42**, 261–283.
52 G. Y. Li, K. L. Huang, Y. R. Jiang, D. L. Yang and P. Ding, *Int. J. Biol. Macromol.*, 2008, **42**, 405–412.
53 F. J. Arriagada and K. J. Osseo-Asare, *J. Colloid Interface Sci.*, 1999, **211**, 210–220.
54 J. Liu, Z. Sun, Y. Deng, Y. Zou, C. Li, X. Guo, L. Xiong, Y. Gao, F. Li and D. Zhao, *Angew. Chem., Int. Ed.*, 2009, **48**, 5875–5879.
55 H. Pan, X. Li, D. Zhang, Y. Guan and P. Wu, *J. Mol. Catal. A: Chem.*, 2013, **277**, 108–114.
56 S. Sayin and M. Yilmaz, *J. Chem. Eng. Data*, 2011, **56**, 2020–2029.
57 Z. C. Li, H. T. Fan, Y. Zhang, M. X. Chen, Z. Y. Yu, X. Q. Cao and T. Sun, *Chem. Eng. J.*, 2011, **171**, 703–710.
58 H. Chen, C. Deng and X. Zhang, *Angew. Chem., Int. Ed.*, 2010, **49**, 607–611.
59 R. Qin, F. Li, M. Chen and W. Jiang, *Appl. Surf. Sci.*, 2009, **256**, 27–32.
60 A. I. Frenkel, C. W. Hills and R. G. Nuzzo, *J. Phys. Chem. B*, 2001, **105**, 12689–12703.
61 G. Neri, C. Milone, S. Galvagno, A. P. J. Pijpers and J. Schwank, *Appl. Catal., A*, 2002, **227**, 105–115.
62 R. Nie, D. Liang, L. Shen, J. Gao, P. Chen and Z. Hou, *Appl. Catal., B*, 2012, **127**, 212–220.
63 Z. Yan, Z. Xu, Z. Yang, L. Yue and L. Huang, *Appl. Surf. Sci.*, 2019, **467–468**, 277–285.
64 J. Wang, S. Zheng, Y. Shao, J. Liu, Z. Xu and D. Zhu, *J. Colloid Interface Sci.*, 2010, **349**, 293–299.
65 F. Ge, M. M. Li, H. Ye and B. X. Zhao, *J. Hazard. Mater.*, 2012, **211–212**, 366–372.
66 C. J. Tan and Y. W. Tong, *Anal. Chem.*, 2007, **79**, 299–306.
67 D. Peng, Y. Zhang, X. Du, L. Zhang, X. Leng, M. D. Walter and Z. Huang, *J. Am. Chem. Soc.*, 2013, **135**, 19154–19166.
68 W. Hu, H. Xie, H. Yue, P. Prinsen and R. Luquee, *Catal. Commun.*, 2017, **97**, 51–55.
69 C. C. H. Atienza, T. Diao, K. J. Weller, S. A. Nye, K. M. Lewis, J. G. P. Delis, J. L. Boyer, A. K. Roy and P. J. Chirik, *J. Am. Chem. Soc.*, 2014, **136**, 12108–12118.
70 I. Buslov, F. Song and X. Hu, *Angew. Chem., Int. Ed.*, 2016, **55**, 12295–12299.
71 A. Vasseur, J. Bruffaerts and I. Marek, *Nat. Chem.*, 2016, **8**, 209–219.
72 R. Ciriminna, V. Pandarus, G. Gingras, F. Béland and M. Pagliaro, *ACS Sustainable Chem. Eng.*, 2013, **1**, 249–253.
73 E. A. Chernyshev, Z. V. Belyakova, L. K. Knyazeva and N. N. Khromykh, *Russ. J. Gen. Chem.*, 2007, **77**, 55–61.